




A re-transmitted chipless tag using CSRR coupled structure

Zhong-Hua Ma^{1,2} · Jian-Hong Yang¹ · Chih-Cheng Chen²  · Cheng-Fu Yang³

Received: 11 February 2018 / Accepted: 5 March 2018 / Published online: 2 April 2018
© The Author(s) 2018

Abstract

To reduce the cost of the traditional RFID tags, a re-transmitted chipless tag based on high Q CSRR structure working on UWB frequency band is proposed, which is composed of two orthogonal polarization transmitting and receiving microstrip broadband monopole antennas, loaded with multiple CSRR resonators. Data encoding is utilized the hybrid encoding technology by the significantly spectral signature of the high-Q CSRR resonator and the different amplitude on the same frequency point. The coding capacity is achieved 84 bits, which is far greater than other structures chipless tag. Several typical re-transmitted chipless tags based on CSRR structure are designed by HFSS software. The results of simulation and test are well agreeable to verify the feasibility of the proposed tag such tag, and it has low cost, narrow bandwidth and compact structure. It can be applied to low-cost logistics, production line management and other fields.

1 Introduction

Radio frequency identification can make automatic identification and tracking of objects through data wireless capture. Carriers carried by data are called tags and transponders. A radio frequency identification (RFID) reader transmits continuous wave (CW) to a tag. The tag capturing the energy of CW is aroused, and then reflects the data back to the reader (Islam et al. 2015) by a tag antenna. With the rapid development of Internet of Things technology, RFID technology has been deeply applied to people's daily life. RFID tags have the potential to replace bar codes, but cost of traditional RFID tags with chips are high compared to bar codes, thus limiting the widespread

use of RFID technology. To apply RFID tags to items with low price, cost of traditional tag must be reduced, while the cost of traditional tag depends mainly on the cost of chips. To compare the cost of traditional tag with that of bar codes, many scholars have proposed chipless tag (Liu and Yao 2008; Vena et al. 2012), which removes the chip of the traditional tag and embeds encoded data in the passive circuit. On the one hand, it highlights the similar features of low cost of bar codes; on the other hand, it also has the characteristics of automatic tracking of traditional tag and long-range automatic identification. Chipless tags mainly consist of time-domain chipless tags (Vemagiri et al. 2007; Liu and Yao 2008; Preradovic and Karmakar 2010; Chamarti and Varahramyan 2006), frequency-domain chipless tags (Balbin and Karmakar 2009; Costa et al. 2013, 2016), hybrid domain chipless tags (Vena et al. 2013; Ni et al. 2017), and space domain chipless tags (Feng et al. 2015).

The time-domain chipless tag is mainly composed of surface acoustic wave (SAW) or micro strip transmission lines (Liu and Yao 2008; Chamarti and Varahramyan 2006). The reader sends a pulse interrogating signal to the tag, and receives pulse echo of backward scattering. The transmission line on the tag delays the back-scatter signal time. This pulse sequence created can be used for data encoding. For encoding the data in the time domain, the tag antenna receives interrogating signal transmitted by the reader and then forms a pulse-code modulated signal via the SAW medium. But it uses high-cost piezoelectric materials. This kind of tag needs submicron photolithography technology, whose cost has been nearly equal to

✉ Jian-Hong Yang
yangjh@lzu.edu.cn

✉ Chih-Cheng Chen
201761000018@jmu.edu.cn; 3343033397@qq.com

Zhong-Hua Ma
mzhxm@jmu.edu.cn

Cheng-Fu Yang
cfyang@nuk.edu.tw

¹ College of Physical Science and Technology, Lanzhou University, Lanzhou 730000, Gansu, China

² School of Information Engineering, Jimei University, Xiamen 361021, Fujian, China

³ Department of Chemical and Material Engineering, National University of Kaohsiung, Kaohsiung 811, Taiwan

traditional tag with chips. The non-flat tag can not be completely printed. Because ID generation circuit based on time-domain transmission delay line does not have chip tags, input signal and delay signal are formed a binary coded signal. The tag volume is relatively much larger, but encoding capacity is smaller.

A large number of documents have reported chipless tag based on spectral features (Ei-Awamry et al. 2015; Balbin and Karmakar 2009; Nijas et al. 2012; Costa et al. 2013, 2016). The encoding is achieved by changing spectral structure of resonators. The resonator is a planar printable structure. Data bits corresponded by each resonator are compared to the output spectrum in the specific resonant frequency. By adding or removing different resonators, the notch of resonance frequency spectrum appears on the spectrum or the notch of the resonance frequency spectrum disappears, which forms information coding of the frequency domain. Coding capacity of frequency-based coding technology is large due to the use of planar circuit technology. It can be printed directly and make mass production. But it occupies a wide spectrum, ultra-wide band dedicated RFID reader is necessary.

Chipless tags based on the AM phase domain (Vena et al. 2013) are encoded using a scatter antenna with microstrip branches. The amplitude of the back scatter signal at each resonant frequency is varied by changing stub width. However, the amplitude resolution is chosen as 1, 1.5 and 2 dB, with a difference of only 0.5 dB. It is relatively low, leading to harsh requests for the inspection environment. It proposes a chipless tag in the document (Ni et al. 2017) based on mixed modulation of amplitude and frequency-domain features. By varying the size of the resonator load, the amplitude of spectral features at each resonant frequency is changed. The amplitude modulation and frequency spectrum characteristics are combined for mixed coding. Coding capacity increases greatly. However, the resolution of amplitude is easily affected by the surrounding environment, which easily causes error codes and harsh requirements on the practical use.

In literature (Feng et al. 2015), it proposed a chipless tag based on spatial angle coding. The scatter is designed into a V-shape. The angle between two arms of the V-shape is determined by measuring the field strength of the orthogonal direction. Then the encoding is performed. Although this chipless tag improves the coding capacity, it is limited by field measurement accuracy and environment. It will have a higher bit error rate in practice.

In this paper, we propose a retransmitted chipless tag on frequency domain, which constitutes by complementary split ring resonator (CSRR) and the transmit-and-receive antennas with orthogonal polarization. The main transmission microstrip line is coupling the unit of the CSRR. The orthogonal transmitting and receiving antennas are

mainly designed to prevent interference between the interrogation signal and the backscatter signal. The CSRR structure has a resonant structure with high quality factor in the RF microwave frequency band (Falcone et al. 2004), which is applicable to the design of a chipless tag based on frequency domain coding. This chipless tag easily adheres to plastic and paper, has a very compact frequency bandwidth. It significantly improves the band utilization and performance, suitable for large-scale use of low-cost items. In the future it can replace bar codes in the field of supermarkets, production lines and logistics.

2 Working principles of retransmitted RFID chipless tag

Figure 1 shows the working principle of a retransmitted chipless tag RFID system based on a coupled CSRR structure proposed in this paper. The reader transmits an ultra-wide band excitation signal with a uniform power spectrum. The CSRR chipless tag is connected to an ultra-wide band antenna. Receiving antenna of tags keeps in line polarization characteristics with transmit antenna of reader. The other transmitting antenna of tag and receiving antenna of tag are orthogonal to each other, which serves as a polarization isolation. Receiving antenna of the reader should be consistent with the polarization characteristics of transmitting antenna of tags. So the ultra-wide band spectrum with the uniform power super broadband signal, which is coupled by the microstrip transmission line changes ultra-wide frequency spectrum of the output. Coding information of tags is embedded in the output spectrum. When readers receive retransmitted signal sent by tags, encoded state will be achieved.

3 Band stop CSRR cell circuit model and characteristics

The structure of complementary split ring resonator was originally proposed by Pendry et al. (1999). Later, the split ring resonator was used in the design of high Q band stop filters (Mustafa et al. 2010). By adding the number of CSRRs with the same size, the bandwidth and resistance characteristics are improved. Because CSRR resonators have very high Q values, they have a smaller bandwidth than other types of resonators, such as helical and C-type resonators. In this paper, it is applied to chipless tag design based on frequency domain coding to improve the spectrum utilization and increase the coding capacity.

Figure 2 is a structural schematic diagram of a retransmitted chipless tag with different side length of rectangular CSRR coupled microstrip transmission lines. The property

Fig. 1 Working principle of the retransmission chipless tag based on CSRR

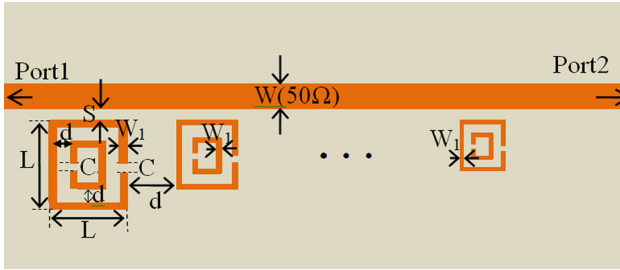


Fig. 2 Structure diagram of chipless tag with CSRR resonator

impedance of microstrip transmission line is 50Ω and the corresponding width is W . All CSRR structures distance micro strip transmission line is S . The microstrip line widths of the inner and outer rings are W_1 . The lengths of the inner and outer split ring openings and their gap are C and d respectively. The distance of adjacent CSRRs is d_1 . The side length of the outer ring of rectangle CSRR is L , and the back of the substrate board has a ground plane. Port 1 and port 2 are connected two orthogonal UWB antennas respectively.

Figure 3 shows equivalent circuit of the microstrip coupled CSRR. L_1 indicates the on-line equivalent inductance of the main transmission. The larger the L_1 is, the greater the signal loss is. That is, when the main transmission microstrip line is much more narrow, attenuation of the line pair signal is much greater. C_{11} represents the degree of coupling between the microstrip line and the CSRR. The smaller the distance between them, the larger the coupling will be. Resonance frequency is affected to move to the low frequency. C_{2n} and L_{2n} are equivalent components of a complementary open-ended resonant microstrip loop, mainly determining the band-stop resonant frequency (Romero et al. 2015). The resonance frequency of a CSRR unit is mainly determined by $\omega = 1/\sqrt{L_2 C_2}$ (Bilotti et al. 2007), and

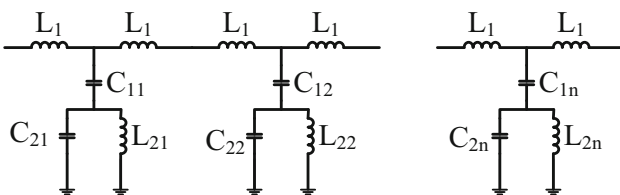


Fig. 3 Equivalent circuits of microstrip coupled CSRR resonators

$$C_2 = C_0[L + 3(d + w_1)/2]. \tag{1}$$

L is the CSRR side length, and d is space of the CSRR inner and outer rings. C_0 is the capacitance of unit length of the two split ring.

$$L_2 = \frac{\mu_0 l_{avg}}{2} \frac{4.86}{4} \left[\ln\left(\frac{0.98}{\rho}\right) + 1.84\rho \right] \tag{2}$$

where $\rho = \frac{w_1+d}{L-w_1-d}$ is the filling factor, $l_{avg} = 8\left[\frac{L}{2} - \frac{(w_1+d)}{2}\right]$

$$C_0 = \epsilon_0 \frac{K(\sqrt{1-k^2})}{K(k)}, \tag{3}$$

wherein $K(k)$ is the first complete elliptic integral, including

$$k = \frac{d/2}{w_1 + d/2} \tag{4}$$

Retransmitted chipless tags are designed and simulated by using the High Frequency Structure Simulator (HFSS), a three-dimensional electromagnetic field simulation software. A Rogers4350 dielectric substrate is used with a relative dielectric constant of 3.66, a loss tangent of 0.004, and a thickness of 0.508 mm. Figure 4 studies characteristics of the scattering parameters when the spacing S of a single CSRR and microstrip transmission line coupling structure equals 0.1 mm. When side length L of CSRR is 6 mm, a band-stop resonance characteristic is formed at about 4.07 GHz. The transmission coefficient $S(2,1)$ is about -20 dB and reflection coefficient $S(1,1)$ is 0 dB. Value of U-type resonator proposed in (Casula et al. 2014) ($S(2,1) = -8$ dB, $S(1,1) = -5$ dB). CSRR has a very high quality factor-about 31.3. It occupies a small

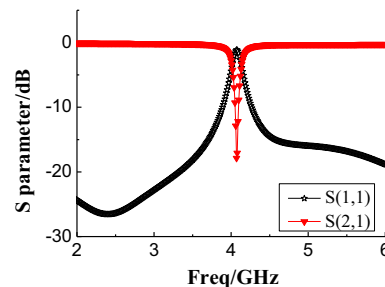


Fig. 4 S parameters of single CSRR couple unit

bandwidth that is ideally suited as a band stop resonant unit with chipless tags.

Figure 5 is a curve of $S(2,1)$ when the side length L of the micro strip of the outer ring of the CSRR unit changes. It can be concluded that with the increase of the side length, the band-stop resonance point decreases. It can be seen from the figure that changing the value of the length L of the CSRR can greatly change the resonance frequency. However, notch depth formed by $S(2,1)$ remains basically constant and the band width of the band-stop impedance is substantially unchanged. When decoding the chipless tag, threshold setting is simple without error code.

Figure 6 shows the CSRR band-stop resonance characteristics when a CSRR band-stop resonator unit and signal transmission microstrip line spacing S changes. When S is larger than 0.4 mm, its notch depth becomes shallower, which indicates that the coupling reduces. The resonance frequency decreases. When S is less than 0.4 mm, the coupling effect is strengthened and the notch depth enhances, sensitivity increases, and the resonance frequency changes slightly. Therefore, the relationship between processing accuracy and spectral sensitivity should be taken into account in designing.

4 Band-stop CSRR chip tag coding and simulation

According to band-stop transmission characteristics of CSRR, CSRR resonators with different lengths are placed on the side of a 50Ω characteristic impedance micro strip transmission line. Each CSRR band-stop resonator corresponds to a resonance frequency in the spectrum. The resonance frequency corresponds to a logic “1” state. When corresponding CSRR resonator is removed, the resonant frequency disappears, it turns to “0”. The structure is shown in Fig. 2. HFSS software is made use of for

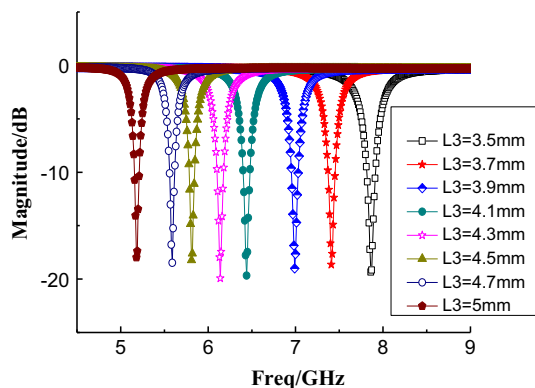


Fig. 5 Relationship of CRSS side length and resonant frequency with $W_1 = 0.5$ mm

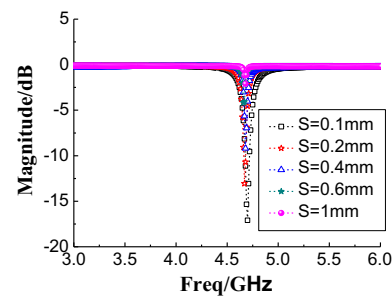


Fig. 6 Resonance point amplitude when the spacing S varies

simulation and optimization. Final corresponding parameter values are shown in Table 1.

When the length of CSRR varies from 6 to 4.8 mm with a step size of 0.2 mm, a combined state of 6 resonators is obtained with $2^6 = 64$ possible combinations. ID is 111111 of the tag when 6 resonators exist, ID of the tag is 000000 when all 6 resonators are removed. Several typical code tags are selected for simulation to obtain the spectrum curves of chipless tag $S(2,1)$ with encoding 111111, 101010, 010101, 110011 and 111000 as shown in Fig. 7. Table 2 shows the resonant frequencies of five different codes with the tag status “1”. The maximum error of each code of the first resonance point is 20 MHz. The maximum error of the second resonance point is 30 MHz, and the maximum error of the third resonance point is 60 MHz. The maximum error of the fourth resonance point is 10 MHz. The maximum error of the fifth resonance point is 40 MHz, and the maximum error of the sixth resonance point is 20 MHz. Considering the error code, the resonance frequency gap of adjacent CSRR resonators must be greater than 60 MHz.

Based on the maximum bandwidth of 60 MHz occupied by each resonator, the protection bandwidth of the two adjacent spectral notch is set to 90 MHz. One spectral feature occupies a bandwidth of 150 MHz. The distance from single CSRR resonator to second harmonic distance is 4.2 GHz, at which 28-bit encoding is possible. As Fig. 6 shows, changing the space of the CSRR and the main microstrip transmission line will lead to change of the notch depth of the resonance point. Their resonant frequencies vary from 4.67 to 4.7 GHz with an occupied frequency band of 30 MHz. The maximum occupied bandwidth is 60 MHz for each resonator. We assume that the frequency remains constant when the coupling distance

Table 1 The value of the structure parameter

Parameters	W	L	c	d	d1	h
mm	1.07	6	0.5	0.5	2	0.508

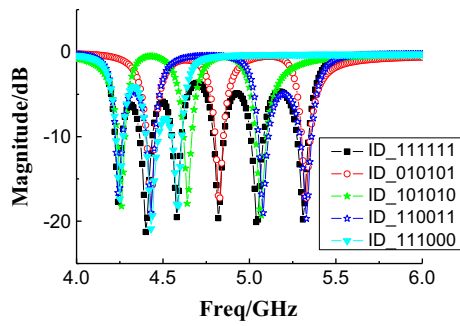


Fig. 7 Simulation results of different CRSS combinations of the six-bit

changes (ie, the notch depth changes). Selective spacing is 0.1, 0.2 and 0.4 mm. When $s = 0.4$ mm, $S_{21} = -9.2$ dB; $S_{21} = -13.1$ dB for $s = 0.2$ mm; $S_{21} = -17.1$ dB for $s = 0.1$ mm. When the space is different, the depth of notch is obviously different with a difference of about 4 dB. Depth of the three notches can be clearly distinguished. There are a total of three different depths of notch. when hybrid coding technology is applied mixed with magnitude modulation and frequency position, CSRR coding capacity becomes $28 \times 3 = 84$ bits. The coding capacity will increase significantly. It is expected that all encoding states will reach 2^{84} states with a huge coding capacity.

5 Ultra-broadband antenna design

The ultra-wide band antenna proposed in Chami et al. (2014) has a compact structure and a wide operating frequency band, which is very suitable for a chipless tag antenna. Based on this structure, another ultra-broadband antenna is designed as shown in Fig. 8 by this paper. The Rogers4350 dielectric substrate is adopted with 0.508 mm of substrate thickness, 36 mm of length and 23 mm of width. The width of feed line W_3 is 1.07 mm, and the length of feed line L_{feed} is 17.5 mm. The gap length on both sides is 2 mm. The width is 0.5 mm.

Figure 9 shows three-dimensional pattern of the UWB antenna. The measured and simulated return loss curves are shown in Fig. 10. When simulated return loss is less than

- 10 dB, the frequency range is between 2.21 to 13.94 GHz, and the bandwidth is 11.73 GHz. When the measured return loss is less than - 10 dB, the frequency range is between 2.83 and 13.45 GHz, and the bandwidth is 10.64 GHz. Simulated and measured ones can meet the work frequency band of chipless tags. Figure 11 is a simulation curve of the voltage standing wave ratio (VSWR) of an ultra-broadband antenna with frequency bands from 2.67 to 13.52 GHz with VSWR less than 2. It completely covers spectrum range of chipless tags used for chipless tag reader and its transceiver antenna.

The gain curve of the UWB antenna is shown in Fig. 12, with omnidirectional radiation on E plane and broadside radiation on H plane. A maximum gain reaches 0.56 dBi for E plane at 4 GHz. The maximum gain of E plane is 2.54 dBi at 8 GHz.

6 Measurement results

According to multi-CSRR band-stop resonator chipless tag in Fig. 2, several typical encoded chipless tag photo made on Rogers4350 substrate are shown in Fig. 13, respectively



Fig. 8 Ultra-wideband antenna photo

Table 2 Resonance frequency corresponding to different coding status

Encoding state	ID_111111 (GHz)	ID_010101 (GHz)	ID_101010 (GHz)	ID_110011 (GHz)	ID_111000 (GHz)
First resonance point	4.24	–	4.26	4.24	4.25
Second resonance point	4.40	4.43	–	4.43	4.43
Third resonance point	4.58	–	4.64	–	4.59
Fourth resonance point	4.82	4.83	–	–	–
Fifth resonance point	5.04	–	5.07	5.08	–
Sixth resonance point	5.31	5.33	–	5.33	–

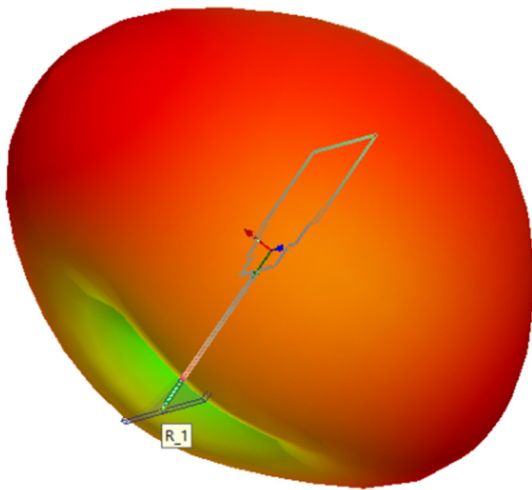


Fig. 9 3D pattern of UWB antenna

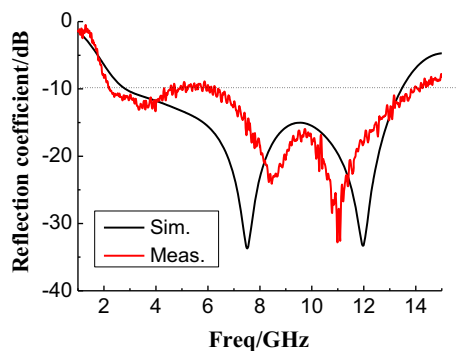


Fig. 10 Reflectance coefficient at the UWB antenna input port

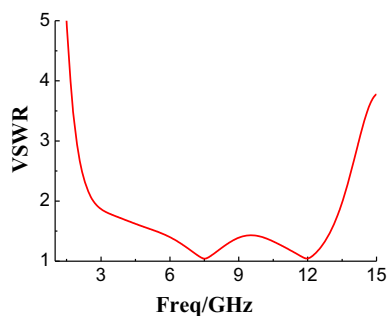


Fig. 11 VSWR of the UWB

ID 111111, ID 010101, ID 110011 and ID 111000. Test system diagram is shown in Fig. 14. A vector network analyzer (Agilent E8362B) takes place of chipless readers. Two orthogonal ultra-broadband antenna is connected to two ports of network analyzers, respectively, as a transmitting antenna and receiving antenna. Transmitting antennas connecting the reader point to the receiving antenna of chipless tag. Receiving antenna connecting the reader is aligned with the transmitting antenna of the chipless tag. Their polarization should be the same. The

horizontal polarization is equal to the horizontal polarization, and the vertical polarization is equal to vertical polarization. Polarization loss should be avoided as much as possible. In order to reduce the interference between readers and Tx–Rx antenna of tags, which should be orthographically polarized to achieve polarization isolation. Distance between reader antenna and the tag antenna is 30 cm.

Figure 15a–d show the simulation and test results of Tag ID 111111, ID 010101, ID 110011 and ID 111000, respectively. There is a 10–40 MHz error in the simulation and measurement of the first resonator corresponding to the resonance point; the 10–60 MHz error exists in the simulation and measurement of the resonance point corresponding to the second resonator; and 10–60 MHz error exists in the simulation and the actual measurement of the resonance point corresponding to the third resonator; 30–70 MHz error exists in the corresponding resonance point of the fourth resonator; the corresponding resonance point of the fifth resonator has an error of 10–40 MHz. The error of simulation and actual measurement of the sixth resonance point is 20–50 MHz. Therefore, as long as the corresponding stop band width of each resonator is controlled within the range of 70 MHz, no interference occurs with each other. No code error occurs during coding and decoding. CSRR chipless tag has a very compact operating frequency band with a bandwidth of only 1.09 GHz for 6 bits of coding capacity, ranging from 4.24 to 5.33 GHz. The magnitude is less than -10 dB at all notches. A -10 dB threshold can be used to differentiate coding states making it easy to identify the states “0” and “1”. Increasing the coding capacity will increase the size of the tag. To miniaturize the size of chipless tag by forming a more compact structure by twisting the 50Ω transmission line or placing the CSRRs on both sides of the 50Ω transmission line.

Table 3 compares features of various types of chipless tags. CSRR-type microstrip coupled chipless tag has higher spectrum utilization and longer communication distance. A detailed comparison of density, transmission dip depth, bits by single resonator, tag antenna gain and read range with our works is presented at Table 4.

7 Discussion

The RO 4350 remains unchanged. The resonant curves of six CSRRs on the tag are shown in Fig. 16 when the thickness of substrate is 0.3, 0.508, and 0.8 mm, respectively. Substrate thickness increases while the frequency of each resonance point decreased slightly. However, it will excite more surface wave mode and increase loss. The CSRR with the smallest length is the most sensitive to

Fig. 12 Gain pattern of UWB antenna **a** 4 GHz, **b** 8 GHz

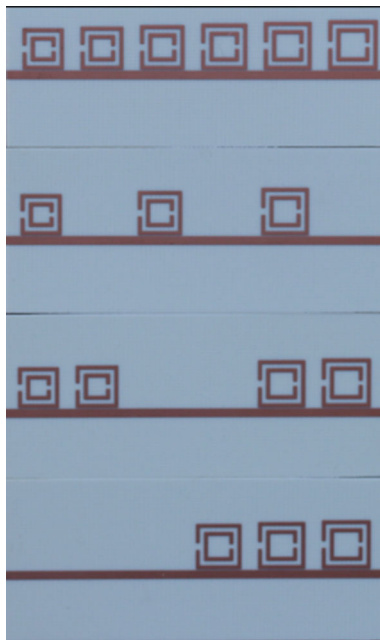
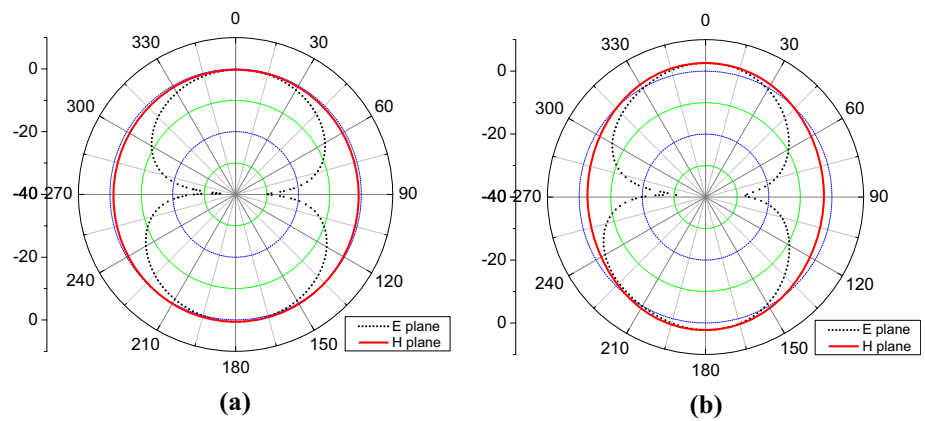


Fig. 13 Photo of CSRR multi-resonator chipless tag

variations in thickness. However, it can be seen from the Fig. 16 that the corresponding resonance frequency can be different in the range of substrate thickness from 0.3 to 0.8 mm. Figure 17 shows the output spectral characteristics of the CSRR when the length of the opening C changes. When CSRR opening length C varies from 0.5 to 1.2 mm, the corresponding band-stop resonance frequency increases, which corresponds to growth of the opening. Equivalent capacitance of C_2 reduces while resonant frequency increases. We can conclude that the size of fine tuning opening can slightly change the band-stop resonance frequency.

When parameters of tag structure remain unchanged in Fig. 13, the substrate is changed to plastic with a relative dielectric constant of 3.1, a loss tangent of 0.008 and a thickness of 1 mm (Haroon et al. 2014). The output spectrum of a 6-bit CSRR chipless tag is shown in

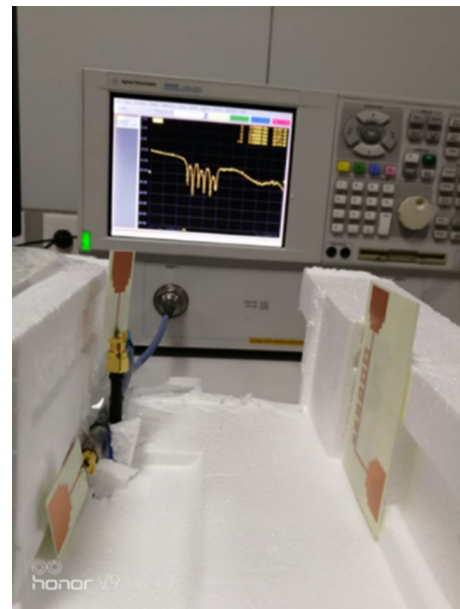


Fig. 14 Diagram of test system

Fig. 18. The output spectrum correctly indicates the encoding status. When the substrate is changed to foam, the relative dielectric constant is 1.06. Loss tangent is 0.0015, and the thickness is also 1 mm (Custodio 2013). The output spectrum of a 6-bit CSRR chipless tag is shown in Fig. 19. Output spectrum can also correctly express coding status.

8 Conclusion

A printable chipless tag has been proposed for a CSRR coupled structure operating in the UWB band and high Q . The tag consists of two orthogonally polarized UWB antennas and a $50\text{-}\Omega$ main signal microstrip transmission line and multiple cascade CSRR structures for different notch frequencies. Each CSRR forms a notch characteristic

Fig. 15 Simulated and measured magnitude for CRSS structure tags with **a** ID 111111, **b** ID 010101, **c** ID 110011, **d** ID 111000

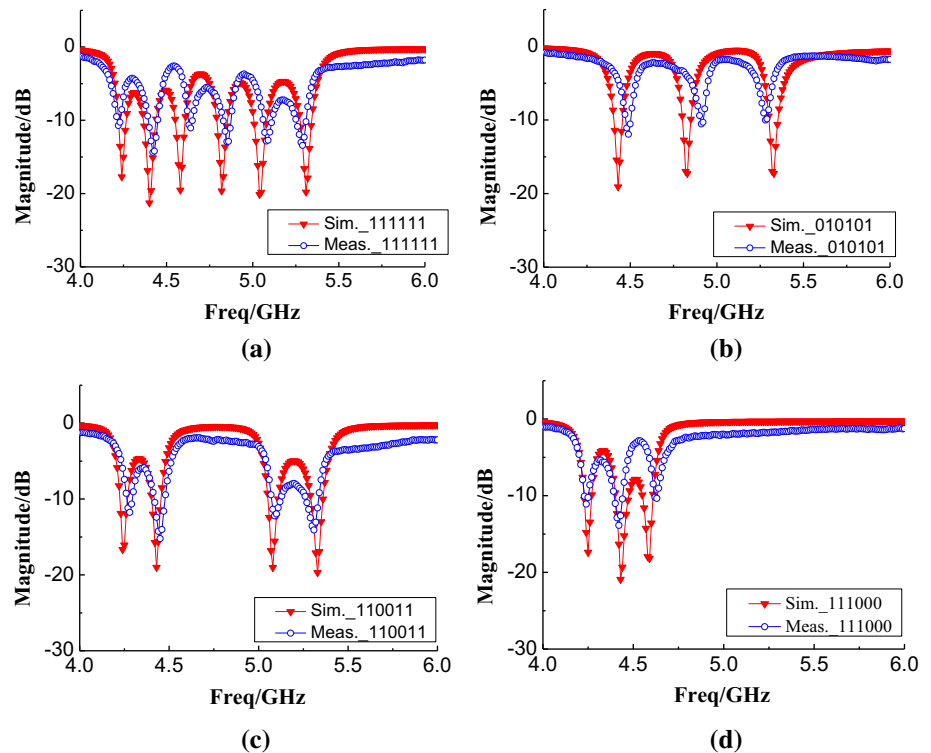


Table 3 Comparison of different structure chipless tag characteristic

Tag resonator	Type	Grounding	Capacity	Read range (cm)
C-type gap (Islam et al. 2012)	RCS	No	1.45 bits/GHz	50
Ring gap (Islam and Karmakar 2012)	RCS	No	2 bits/GHz	20
Rectangular microstrip loop (Costa et al. 2016)	RCS	Yes	1.25 bits/GHz	50–55
Text	Retransmitted	Yes	> 5.5 bits/GHz	30

Table 4 Comparison of different re-transmission chipless tags

Resonator type	Density (bits/cm ²)	Notch depth (dB)	Bits by single resonator	Tag antenna gain (dBi)	Read range (cm)
L-shaped slot DGS (Khaliel et al. 2015)	1.4	– 15 to – 22	0.5	2.3–3	30
SIR stripe (Girbau et al. 2012)	Not specific	– 10 to – 25	1	4	50
Spiral stripe (Preradovic et al. 2009)	0.61	– 5 to – 15	1	2	Not specific
Open stub stripe (Haroon et al. 2013)	0.17	– 17 to – 32	1	2	40
U-shaped (Casula et al. 2014)	0.07	– 9 to – 12	1	3.25	> 50
CSRR (this paper)	0.63	– 10 to – 15	3	1.8–2.5	30

in the spectrum of tag re-transmission, corresponding to one data bit. The proposed tag has a high spectral efficiency and 6-bit encoding is achieved in the frequency band from 4.24 to 5.33 GHz, as shown in Table 3. It has a very high encoding capacity compared to other literature.

Resonator and UWB antenna is designed by 3D CAD software HFSS. Measured results are well matched with simulation results. The proposed tags are suitable for items with low cost, which can replace cheap bar codes.

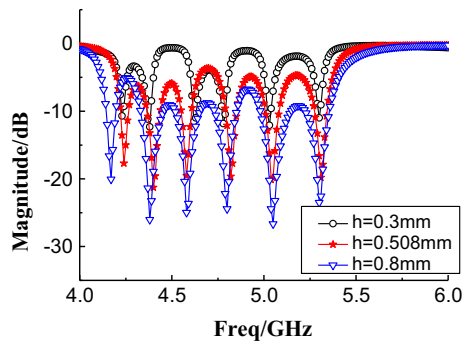


Fig. 16 Substrate thickness changes

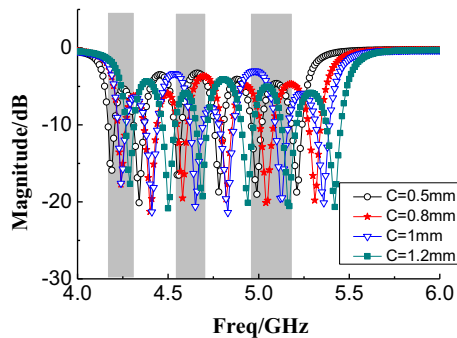


Fig. 17 Change in resonant frequency as the length of C

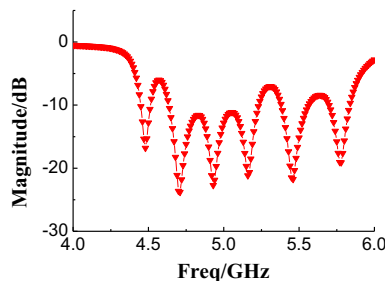


Fig. 18 Dielectric material is plastic

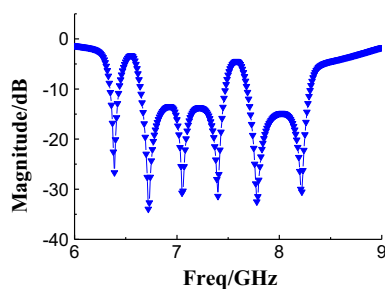


Fig. 19 Dielectric material is foam

Acknowledgements The authors would like to acknowledge the financial support of this project by the Natural Science Foundation of Fujian Province (2015J01657) and the Xiamen Industry-University-Research Collaboration Project (3502Z20163008).

Open Access This article is distributed under the terms of the Creative Commons Attribution 4.0 International License (<http://creativecommons.org/licenses/by/4.0/>), which permits unrestricted use, distribution, and reproduction in any medium, provided you give appropriate credit to the original author(s) and the source, provide a link to the Creative Commons license, and indicate if changes were made.

References

- Balbin I, Karmakar NC (2009) Phase-encoded chipless RFID transponder for large-scale low-cost applications. *IEEE Microw Wirel Compon Lett* 19:509–511
- Bilotti F, Toscano A, Vegni L (2007) Design of spiral and multiple split-ring resonators for the realization of miniaturized metamaterial samples. *IEEE Trans Antennas Propag* 55:2258–2267
- Casula GA, Montisci G, Maxia P et al (2014) A narrowband chipless multiresonator tag for UHF RFID. *J Electromagn Waves Appl* 28:214–227
- Chamarti A, Varahramyan K (2006) Transmission delay line-based ID generation circuit for RFID applications. *IEEE Microw Wirel Compon Lett* 16:588–590
- Chami A, Brachat P, Fortino N et al (2014) Babinet’s principle applied to ultra-wideband antennas for high isolation. *Electron Lett* 50:60–62
- Costa F, Genovesi S, Monorchio A (2013) A chipless RFID based on multiresonant high-impedance surfaces. *IEEE Trans Microw Theory Tech* 61:146–153
- Costa F, Genovesi S, Monorchio A (2016) Normalization-free chipless RFIDs by using dual-polarized interrogation. *IEEE Trans Microw Theory Tech* 64:310–318
- Custodio P (2013) High efficiency aperture-coupled stacked-patch antennas with foam substrate. In: *IEEE antennas and propagation society international symposium (APSURSI 2013)*, Orlando. IEEE, pp 1828–1829
- Ei-Awamry A, Khaliel M, Fawky A et al (2015) Novel notch modulation algorithm for enhancing the chipless RFID tags coding capacity. In: *IEEE international conference on RFID*, San Diego. IEEE, pp 25–31
- Falcone F, Lopetegi T, Baena JD et al (2004) Effective negative- ϵ Stopband microstrip lines based on complementary split ring resonators. *IEEE Microw Wirel Compon Lett* 14:280–282
- Feng CX, Zhang WM, Li L et al (2015) Angle-based chipless RFID tag with high capacity and insensitivity to polarization. *IEEE Trans Antennas Propag* 63:1789–1797
- Girbau D, Lorenzo J, Lazaro A et al (2012) Frequency-coded chipless RFID tag based on dual-band resonators. *IEEE Antennas Wirel Propag Lett* 11:126–128
- Haroon, Ullah S, Flint A (2014) Electro-textile based wearable patch antenna on biodegradable poly lactic acid (PLA) plastic substrate for 2.45 GHz, ISM band applications. In: *International conference on emerging technologies (ICET2014)*, Islamabad. IEEE, pp 158–163
- Islam MA, Karmakar NC (2012) A novel compact printable dual-polarized chipless RFID system. *IEEE Trans Microw Theory Tech* 60:2142–2151
- Islam MA, Karmakar N (2015) A compact printable dual-polarized chipless RFID tag using slot length variation in ‘I’ slot resonators. In: *European microwave conference (EuMC2015)*. IEEE, Paris, pp 7–10
- Islam MA, Yap Y, Karmakar N et al (2012) Orientation independent compact chipless RFID tag. In: *IEEE international conference on RFID-technologies and applications (RFID-TA)*, IEEE, Nice, 5–7 Nov 2012. <https://doi.org/10.1109/RFID-TA.2012.6404499>

- Khaliel M, Ei-Hadidy M, Kaiser T (2015) Printable depolarizing chipless RFID tag based on DGS resonators for suppressing the clutter effects. In: Ninth European conference on antennas and propagation (EuCAP2015), Lisbon. IEEE, pp 1–5
- Liu JC, Yao JH (2008) Wireless RF identification system based on SAW. *IEEE Trans Ind Electron* 55:958–961
- Mustafa K, Al-Nuaimi T, Whittow WG (2010) Compact microstrip band stop filter using SRR and CSSR: design, simulation and results. In: Proceedings of the fourth European conference on antennas and propagation (EuCAP2010), Barcelona. IEEE, pp 1–5
- Ni Y, Huang XD, Lv YP et al (2017) Hybrid coding chipless tag based on impedance loading. *IET Microw Antennas Propag* 17:1325–1331
- Nijas CM, Dinesh R, Deepak U et al (2012) Chipless RFID tag using multiple microstrip open stub resonators. *IEEE Trans Antennas Propag* 60:4429–4432
- Pendry JB, Holden A, Robbins DJ et al (1999) Magnetism from conductors and enhanced nonlinear phenomena. *IEEE Trans Microw Theory Tech* 47:2075–2084
- Preradovic S, Karmakar N (2009) Design of fully printable planar chipless RFID transponder with 35-bit data capacity. In: European microwave conference (ErMC2009), Rome. IEEE, pp 013–016
- Preradovic S, Karmakar NC (2010) Chipless RFID: bar code of the future. *IEEE Microw Mag* 11:87–97
- Romero RA, Feitoza RS, Rambo CR et al (2015) A low-cost passive wireless capacitive sensing tag based on split-ring resonator. In: IEEE international instrumentation and measurement technology conference (I2MTC 2015) proceedings, Pisa. IEEE, pp 434–439
- Vemagiri J, Chamarti A, Agarwal M et al (2007) Transmission line delay-based radio frequency identification (RFID) tag. *Microw Opt Technol Lett* 49:1900–1904
- Vena A, Perret E, Tedjini S (2012) A fully printable chipless RFID tag with detuning correction technique. *IEEE Microw Wirel Compon Lett* 22:209–211
- Vena A, Babar AA, Sydanheimo L et al (2013) A novel near-transparent ASK-reconfigurable inkjet-printed chipless RFID tag. *IEEE Antennas Wirel Propag Lett* 12:753–756